Micromechanics of Pile Cyclic Response in Sand

Ciantia, Matteo

Published in:
Challenges and Innovations in Geomechanics

DOI:
10.1007/978-3-030-64518-2_62

Publication date:
2021

Document Version
Peer reviewed version

Micromechanics of pile cyclic response in sand

Matteo Oryem Ciantia

School of Science and Engineering, University of Dundee,
Perth Road, DD1 4HN, Dundee (UK)
m.o.ciantia@dundee.ac.uk

Abstract A 3D discrete element model is used to investigate the axial cyclic response of a small-scale displacement piles installed in Fontainebleau sand. Calibration chamber experimental results from literature are used to validate the pile penetration phase of the DEM model which is then employed to simulate stress controlled vertical cyclic loading. The crushable DEM particle model is calibrated using high pressure element test data for the same sand. The model predicts the experimental stress measurements surrounding the jacked pile in both penetrating and unloaded conditions. The DEM model is used to assess micromechanical features hard to detect using experimental and continuum numerical methods. Grain crushing within the soil is observed to occur only below the cone during pile penetration. The analysis of particle stresses and force chains highlight how arching develops around the shaft. These arching effects create a sort of shield around the shaft causing the radial stresses to be lower. After pile installation is completed, a numerical parametric study of stress controlled cyclic axial loading of the pile is performed. The results show that depending on the magnitude of the cyclic load *stable* or *metastable* pile cyclic response is attained. The cyclic load amplitude also influences in different ways both stress and density profiles around the pile. These results may serve as a step forward to the understanding of installation effects on axial cyclic performance of jacked piles in sand.

Keywords: piles, cyclic loading, setup, crushing, DEM, sands

1 Introduction

Driven pile design improvements have been gained with effort through approaches such as those set out by Jardine et al. (2005) and Lehane et al. (2005). However, the effective stress regime developed around piles driven in sands and the factors that control features such as their cyclic loading response and pile setup, remain incompletely understood; see Jardine (2019). Experimental research using calibration chambers (CC) (Yang et al., 2010) and model centrifuge tests (Bolton et al., 1999) has highlighted the importance of the intense stress concentrations that develop below pile tips, the sand grains' strength or crushability and the impact of pile geometry and driving cycles on the final stress regime. Penetration tests using instrumented piles and calibration chambers have advanced understanding of ground displacement mechanisms and evolution of stresses in situ (Arshad et al., 2014). Centrifuge modelling of axial cyclic loading of piles reveled

This is a post-peer-review, pre-copyedit version of an article published in *Lecture Notes in Civil Engineering*, vol. 126. The final authenticated version is available online at: https://doi.org/10.1007/978-3-030-64518-2_62.

that pile performance is greatly influenced by installation effects and the type (load or displacement control) of cyclic loading (Li et al., 2010). Tsuha *et al*. (2012) extended the CC experimental campaign of Yang et al., (2010) to axial cyclic loading. In particular, by exploring the local effective stress evolution, the highly instrumented experiments offered new insights into pile capacity degradation processes. Ciantia et al. (2019a) recently showed that the discrete element method (DEM) can be efficiently used to simulate cyclic-jacked pile penetration in sand. In particular a crushable DEM model was able to accurately reproduce the stress distributions measured in Yang et al. (2010) experiments. Inspired by Tsuha *et al*. (2012), in this contribution the DEM crushing model by Ciantia et al (2019a) is used to investigate the cyclic response of the small-scale displacement piles installed in Fontainebleau sand. Numerical simulations of cyclic stress-controlled pile loading, accounting for installation effects, are performed. Particle-scale DEM data provides new insights that advance understanding of the arching which develops around the shaft after penetration. It is shown how the cyclic loading of the pile induces stress and density redistributions around the shaft. The DEM results are in good agreement with the experimental trends by Tsuha *et al*. (2012) and provide insightful micromechanical data that can be used to further interpret the experiments.

2 DEM particle crushing model

The crushable DEM grain model of Ciantia et al. (2015) was employed. The model's particle failure criterion follows Russell et al. (2009). Particles crush when any interparticle contact force reaches the limit

$$F \leq \sigma_{lim} \cdot A_F = \left\{ \sigma_{lim} \pi \left[\frac{3}{4} \left(\frac{1-\nu_1^2}{E_1} + \frac{1-\nu_2^2}{E_2} \right) \Big/ \left(\frac{1}{r_1} + \frac{1}{r_2} \right) \right]^{\frac{2}{3}} \right\}^3 \quad (1)$$

where σ_{lim} is the limit strength of the material and A_F is the contact area which is recast using Hertzian theory for smooth sphere contacts. r_i (i=1,2) are the radii of the contacting spheres and E_i, ν_i are the Young's Moduli and Poisson's ratios respectively. To incorporate experimentally observed grain variability into the model, the limit strength, σ_{lim}, for a given sphere size is assumed to be normally distributed. A particle size dependency is also introduced to capture the relatively higher strength of smaller particles. Once the crushing limit condition is reached, the spherical particles are split into smaller inscribed tangent spheres. The crushing model was implemented in PFC3D (Itasca 2016). The model parameters used in the current study, listed on Table 1 are those obtained in an extensive calibration to match Fontainebleau sand response.

Table 1 Calibrated model parameters for Fontainebleau sand grains (Ciantia et al. 2019b).

d_{50}	μ	G	ν	$\sigma_{lim,0}$	m	d_0	var	d_{comm}	d_{max}	d_{min}	D_{loc}
mm	-	*GPa*	-	*GPa*	-	*mm*	-	-	*mm*	*mm*	-
0.21	0.275	9	0.2	1.9	10	2	0.36	0.11	0.27	0.01	0.05

3 DEM model setup soil initial conditions

Figure 1(a) reports a schematic diagram of the instrumented model pile tests conducted in Grenoble 3S-R calibration chamber, after Jardine (2019). As indicated the DEM model represents only the inner core of the chamber. As detailed in Ciantia et al. (2019a) an upscaling factor of 39 was applied to sand size, maintaining the shape of the Fontainebleau sand particle size distribution curve. This allowed the analyses to proceed with four orders of magnitude fewer particles than in the experiments and led to a computationally feasible initial number of 442,335 particles (Figure 1(b)). In the present analyses the crushing law used is scalable to avoid the unrealistic results possible when scaling is not considered.

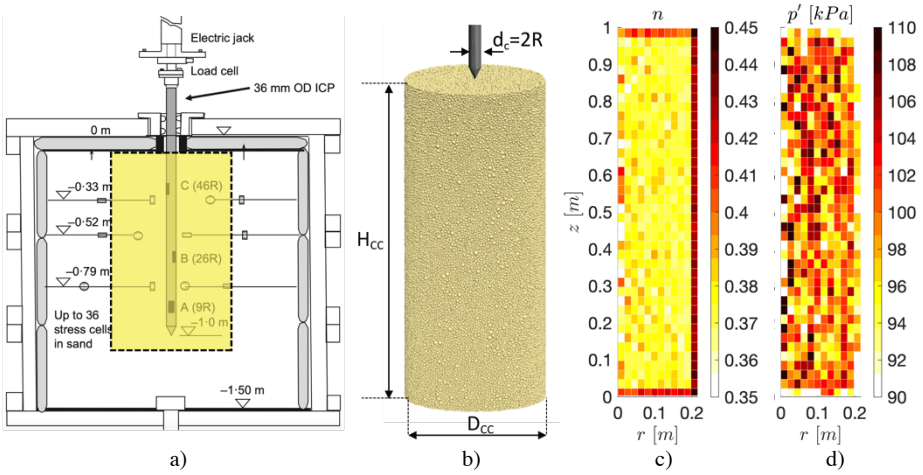

Fig. 1 a) Schematic diagram of experimental CC and region considered for numerical analyses. (b) 3D view of DEM model and corresponding contours of porosity (c) and mean effective stress p' (d).

The calibration chamber (CC) instrumented pile tests were performed under a no-strain, low friction, radial lateral condition. The experimental CC had an initial porosity n=0.382. The DEM CC was filled using the radius expansion method as described by Ciantia et al. (2016, 2018). In the DEM model, the top (frictionless) horizontal boundary was servo-controlled to apply the experimental vertical stress level (150 kPa) while both the bottom (frictionless) wall was fixed as in the experiment. The exterior horizontal stress was adjusted to match the experimentally observed 76 kPa value by using radial wall servo-control, giving a final average porosity of 0.383 and a mean effective stress p'=101 kPa (Figure 1(c,d)). The pile shaft and tip were modelled using rigid frictional cylindrical walls with the interface friction coefficient set equal to the critical state value (tanδ =0.5) measured in interface ring-shear tests (Yang et al. 2010). The particle-pile contacts employed a simplified Hertz-Mindlin contact model with the pile shear modulus (G_{pile}) and Poisson's ratio (ν_{pile}) set to 85 GPa and 0.2 respectively. After 0.8 m of cuasi-static penetration, the pile was unloaded by slowly displacing it upwards until the pile vertical force (Q) was zero. Figure 2(a) gives the penetration data from the DEM

simulations and the corresponding fitted penetration curve. The steady state pile base resistance Q_b (around 20 kN) matches very well the experimental results. The shaft capacity (Q_s) before unloading is 11 kN while it assumes a value of -6 kN (in tension) at the end of installation. The radial stress regime developed in the sand beneath and above the moving pile matched effectively the experimental results (Ciantia et al 2019a) and Figure 2(b) reports the mean effective stress at the end of pile installation in the 'pause' $Q=0$ conditions while Figure 2(c) shows the corresponding porosity contours. The full set of results, including principal stresses, breakage index and particle displacements related to the installation phase can be found in Ciantia et al. (2019a).

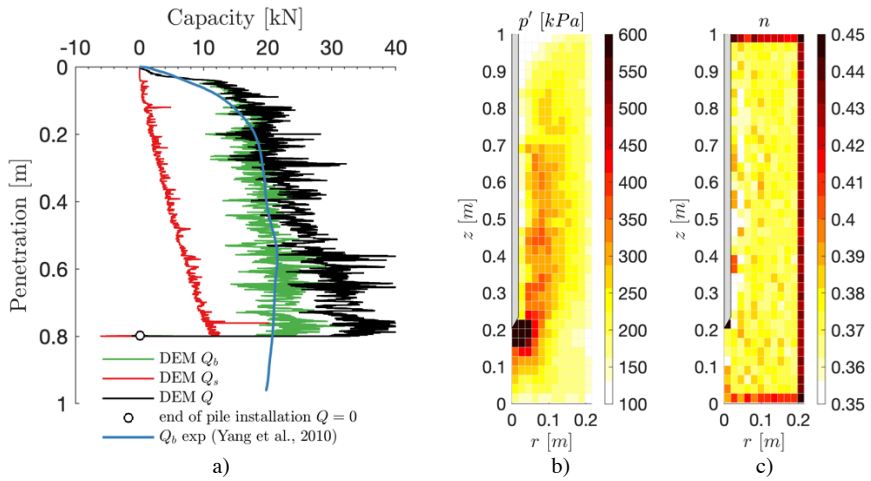

Fig. 2 a) Base (Q_b), shaft (Q_s) and total (Q) pile capacity versus penetration depth. Illustration of mean effective stress (b) and porosity (c) spatial distribution at the end of pile installation (Q = 0 and penetration depth 0.8 m).

3.3 Effect of axial cyclic loading to pile response

To simulate the axial cyclic response of the pile, a cyclic load servo-control was implemented. The vertical force on the pile Q was set to:

$$Q = Q_{mean} + \Delta Q sin(2\pi t/T) \quad (2)$$

where Q_{mean} is the average vertical force while ΔQ is the amplitude of the vertical load cycle and T is the period of the cyclic load. Starting from the unloaded (Q_{mean}=0) conditions and imposing the cycling period to 2000 steps, tests composed by 500 cycles (N_c) considering four loading amplitudes where considered (Table 2).

Table 2 Cyclic axial test cases considered. Q_{mean} = 0 and N_c=500 for all cases

CASE	*A*	*B*	*C*	*D*
ΔQ	500	1000	2000	4000

Figure 3 compares the cyclic response of the pile subject to the 4 different load amplitudes. Cases *A*, *B* and *C* show typical *stable* type of behavior where the axial displacements stabilize or accumulate very slowly with number of cycles. On the other hand, the displacements for case *D* accumulate at moderate rates without stabilising. This is typical of *metastable* behavior (Jardine and Standing 2010). An experimental test very similar to case D was also performed by Tsuha *et al*. (2012). Although the pile penetration depth in the experiment and the DEM model are slightly different (1m and 0.8m respectively) a direct comparison was made (Figure 3(b)). Note that the experimental data was modified to clean a very large initial displacement recorded in the first cycle. Figures 3(c) and (d) show how the base vertical load and shaft resistance evolve as N_c increases. For the metastable behavior (case D) Q_b decreases while Qs slightly increases to maintain the total mean load Q=0. After 500 cycles the base capacity goes to zero and the displacements diverge into a tensile failure.

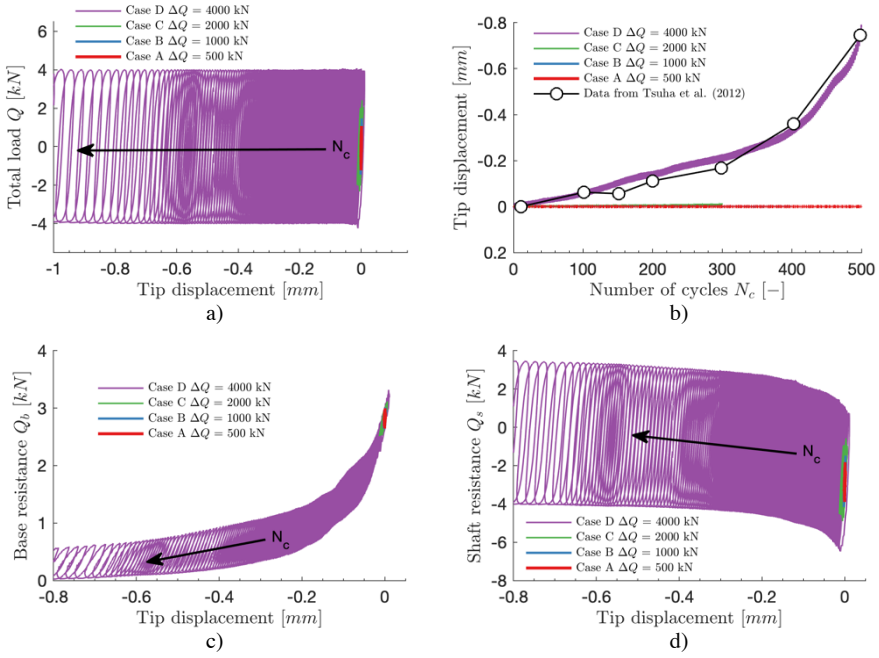

Fig. 3 Comparison of pile cyclic response for the four different cyclic load amplitude cases: a) load penetration, b) pile displacement vs number of cycles. Cyclic loading induced evolution of base (c) and shaft (d) capacity with pile tip displacement.

The decrease of tangential stresses on the shaft is clearly caused by a decrease of radial stresses acting on the shaft. These are represented in Figure 4. For case A, B and C the

radial stress decrease was minimal, while for the metastable case (case D) the mean radial stresses on the shaft decrease until tensile failure of the pile.

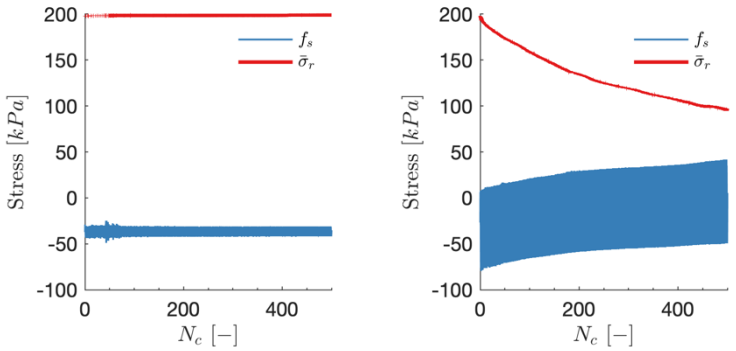

a) CASE A b) CASE D

Fig. 4 Evolution of average tangential (f_s), radial ($\bar{\sigma}_r$) shaft stresses with N_c.

Contours of porosity and mean effective stress changes induced by the axial cyclic loading (N_c=200) are reported in Figure 5. Interestingly for the *stable* cases (A, B and C) densification and stress relaxation are minimal. On the other hand, the *metastable* case shows a decrease in mean effective stress of about 25% (after 200 cycles) around the pile, accompanied by a significant densification (of up to 3.5%) in the vicinity of the shaft.

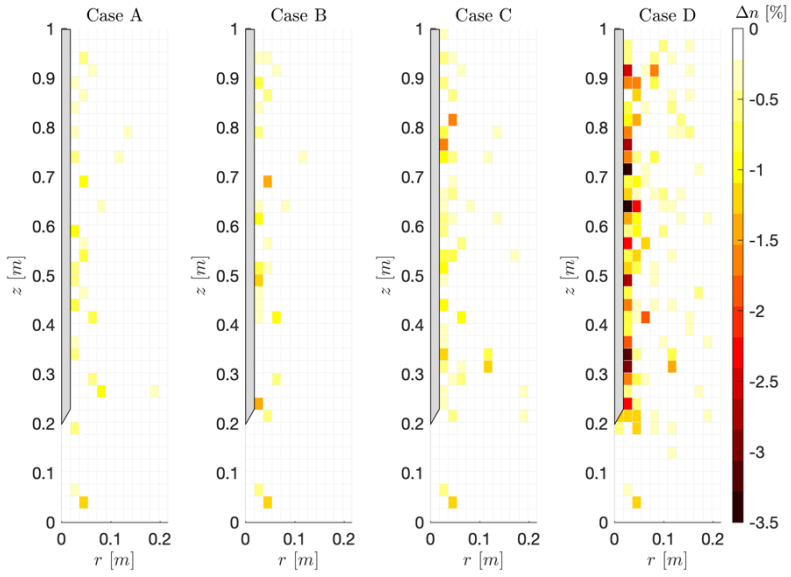

a) porosity change

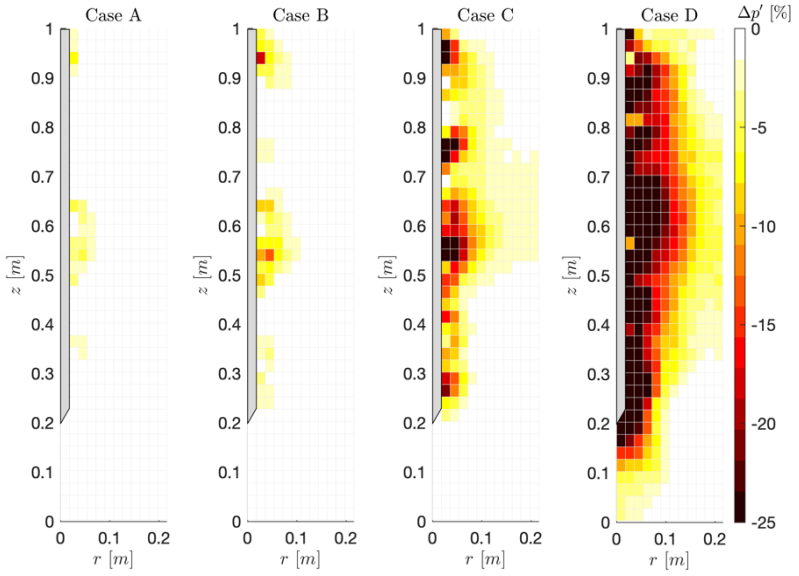

b) mean effective stress change

Fig. 6 Illustration of densification (a) and corresponding mean effective stress relaxation (b) induced by cyclic axial loading of pile.

4 Conclusions

To effectively investigate the axial cyclic loading behavior of piles, installation effects on soil state (i.e. stress and density) should be considered. Ciantia *et al*. (2019a) were able to effectively capture the stress fields around a displacement pile using a large-scale DEM model replicating Yang et al. (2010) CC experiments. The same CC setup was later used by Tsuha *et al*. (2012) to experimentally investigate the axial cyclic performance of the same piles after installation. In this paper the Ciantia *et al*. (2019a) DEM CC model was extended to perform load controlled axial cyclic loading of the jacked pile. The model results are again in good agreement with the physical experiment. As observed experimentally the amplitude of the cyclic load and number of cycles may cause a *stable*, *metastable* and *unstable* pile response. The DEM simulations presented offer new insights into the behavior of piles under cyclic loading, for instance the unexpected connection between stress relaxation and densification around the shaft. A micromechanical investigation is needed to clarify that connection. Finally, it is worth noting that the crushable DEM model employed to reproduce such a complex behaviour was calibrated using generic single particle crushing data and a single high pressure oedometer.

References

Arshad, M.I., Tehrani, F.S., Prezzi, M., Salgado, R., (2014). Experimental study of cone penetration in silica sand using digital image correlation. *Géotechnique* **64**, 551–569.

Bolton, M.D., Gui, M.W., Garnier, J., Corte, J.F., Bagge, G., Laue, J., Renzi, R., (1999). Centrifuge cone penetration tests in sand. *Géotechnique* **49**, 543–552.

Ciantia, M.O., Arroyo, M., Calvetti, F., Gens, A., (2015). An approach to enhance efficiency of DEM modelling of soils with crushable grains. *Géotechnique* **65**, 91–110.

Ciantia, M.O., Arroyo, M., Butlanska, J., Gens, A., (2016). DEM modelling of cone penetration tests in a double-porosity crushable granular material. *Comput. Geotech.* **73**, 109–127.

Ciantia, M.O., Boschi, K., Shire, T., Emam, S., (2018). Numerical techniques for fast generation of large discrete-element models. *Proc. Inst. Civ. Eng. - Eng. Comput. Mech.* **171**(4), 147–161.

Ciantia, M.O., O'Sullivan, C., Jardine, R.J., (2019a). Pile penetration in crushable soils: Insights from micromechanical modelling. In: Proceedings of the XVII ECSMGE-2019. Reykjavík, pp. 298–317.

Ciantia, M.O., Arroyo, M., O'Sullivan, C., Gens, A., Liu, T., (2019b). Grading evolution and critical state in a discrete numerical model of Fontainebleau sand. *Géotechnique* **69**(1), 1–15. https://doi.org/10.1680/jgeot.17.P.023

Itasca, C.G.I., (2016). Particle Flow Code, V. 5.0.

Jardine, R.J., Chow, FC, Overy, RF and Standing, J.R., (2005). *ICP design methods for driven piles in sands and clays*". Thomas Telford Ltd, London p. 105.

Jardine, R.J., Standing J.R, (2012). Field axial cyclic loading experiments on piles driven in sand. So*ils and Foundations* **52**(4):723–736

Jardine, R.J., Zhu, B.T., Foray, P., Yang, Z.X., (2013). Measurement of stresses around closed-ended displacement piles in sand. *Géotechnique* **63**, 1–17.

Jardine, R.J., (2019). Geotechnics, Energy and Climate Change. 56th Rankine Lecture, *Géotechnique*.https://doi.org/10.1680/jgeot.18.RL.001

Lehane, B.M., Schneider, J.A., Xu, X., (2005). A review of design methods for offshore driven piles in siliceous sand. UWA Rep. GEO 5358.

Li Z., Haigh S K., Bolton M D. (2010). The Behavior of a Single Pile under Cyclic Axial Loads. *Deep Foundations and Geotechnical In Situ Testing*. Proceedings. https://doi.org/doi:10.1061/41106(379)17

Russell, A.R., Muir Wood, D., Kikumoto, M., (2009). Crushing of particles in idealised granular assemblies. *J. Mech. Phys. Solids* **57**, 1293–1313.

Tsuha, C. H.C., Foray P. Y., Jardine R. J., Yang Z. X., Silva M., Rimoy S. (2012). Behaviour of Displacement Piles in Sand under Cyclic Axial Loading. S*oils and Foundations* **52** (3): 393–410. https://doi.org/10.1016/j.sandf.2012.05.002

Yang, Z.X., Jardine, R.J., Zhu, B.T., Foray, P., Tsuha, C.H.C., (2010). Sand grain crushing and interface shearing during displacement pile installation in sand. *Géotechnique* **60**, 469–482.